Solvent Study of the Kinetics of Molybdenum Radical Self-Termination

John C. Linehan,*,† Clement R. Yonker,† R. Shane Addleman,† S. Thomas Autrey,† J. Timothy Bays,‡ Thomas E. Bitterwolf,§ and John L. Daschbach†

Pacific Northwest National Laboratory, P.O. Box 999, Richland, Washington 99352, Chemistry Department, United States Military Academy, West Point, New York, and The Department of Chemistry, University of Idaho, Moscow, Idaho 83844

Received August 18, 2000

The kinetics of (*n*-butylCp)Mo(CO)$_3$ (*n*-butylCp is *n*-butyl-η^5-cyclopentadienyl) radical self-termination to form a nonequilibrium mixture of *trans*- and *gauche*-[(*n*-butylCp)Mo(CO)$_3$]$_2$ and the kinetics of the *gauche*-to-trans isomerization have been determined in the liquid solvents *n*-heptane, tetrahydrofuran, xenon (350 bar), and CO_2 (350 bar) at 283 K by step-scan FTIR spectroscopy. The overall rate constant for the disappearance, $2k_R$, of the (*n*-butylCp)Mo(CO)$_3$ radical increases with decreasing solvent viscosity as expected, except in CO_2, which is anomalously slower. The slower overall termination rate in liquid CO_2 is consistent with the formation of a transient molybdenum radical−CO_2 complex. The observed overall rate constants for (*n*-butylCp)Mo(CO)$_3$ self-termination, $2k_R$, are $(7.9 \pm 0.5) \times 10^9$ M^{-1} s^{-1} in xenon; $(3.2 \pm 0.5) \times 10^9$ M^{-1} s^{-1} in heptane; $(2.2 \pm 0.8) \times 10^9$ M^{-1} s^{-1} in THF; and $(1.7 \pm 0.5) \times 10^9$ M^{-1} s^{-1} in CO_2. The first determinations of the radical self-termination-to-*gauche* rate constants, k_G, are presented. The values of k_G are much slower than the corresponding recombination to trans, k_T, reflecting a steric contribution to the rate. The rate of isomerization (rotation about the molydenum−molybdenum bond) from *gauche* to trans is unaffected by the solvent and is 3 times faster than the reported isomerization rate for the nonsubstituted [CpMo(CO)$_3$]$_2$ molecule.

Introduction

The photolytic chemistry of [CpM(CO)$_3$]$_2$ (Cp is η^5-cyclopentadienyl, M is Cr, Mo, W) has been well studied.[1−5] Photolysis of these metal−metal dimers can lead to carbonyl loss with UV photons to produce a pentacarbonyl intermediate which can then add another ligand, recombine with the displaced carbonyl, or lose a second carbonyl to produce a stable tetracarbonyl species. In contrast visible irradiation leads almost exclusively to metal−metal bond scission to produce the CpM(CO)$_3$ radical.[6,7] The metal radical can react to reform the dimer, abstract an atom or group from a substrate, or disproportionate. Rates of CpM(CO)$_3$ recombination, rates of atom abstraction by CpM(CO)$_3$, and the possible solvent effects on cage recombination rates/cage radical escape have all been reported.[8−10]

Early research has shown that there are two isomers of [CpM(CO)$_3$]$_2$ in solution, a *gauche* rotamer in which the cyclopentadienyl rings are adjacent and a *trans* rotamer in which the cyclopentadienyl rings are far removed from each other, as shown in Figure 1. The equilibrium constant between these two rotamers varies proportionally with the dielectric constant of the solvent. The proportion of the *gauche* isomer increases with increasing solvent dielectric constant.[11,12] Recent work has shown that the recombination of CpMo(CO)$_3$ radicals leads to formation of both the *gauche* and *trans* rotamers, but the rate constant for the formation of the *gauche* rotamer from the radical has not been reported.[6,7]

Continuing our interest in the study of organometallic chemistry in compressible fluids[13,14] and our interests in organic/organometallic radical chemistry,[15−17] we

† Pacific Northwest National Laboratory.
‡ United States Military Academy.
§ University of Idaho.

(1) Atruc, D. *Electron Transfer and Radical Processes in Transition-Metal Chemistry*; VCH Publishers: New York, 1995.
(2) Meyer, T. J.; Caspar, J. V. *Chem. Rev.* **1985**, *85*, 187−218.
(3) Tyler, D. R. *Prog. Inorg. Chem.* **1988**, *36*, 125−194.
(4) Tyler, D. R. *Acc. Chem. Res.* **1991**, *24*, 325−331.
(5) Trogler, W. C. *Organometallic Radical Processes*; Elsevier: Amsterdam, 1990; Vol. 22.
(6) Peters, J.; George, M. W.; Turner, J. J. *Organometallics* **1995**, *14*, 1503−1506.
(7) Knorr, J. R.; Brown, T. L. *J. Am. Chem. Soc.* **1993**, *115*, 4087−4092.
(8) Male, J. L.; Lindfors, B. E.; Covert, K. J.; Tyler, D. R. *Macromolecules* **1997**, *30*, 6404−6406.
(9) Male, J. L.; Lindfors, B. E.; Covert, K. J.; Tyler, D. R. *J. Am. Chem. Soc.* **1998**, *120*, 13176.
(10) Male, J. L.; Yoon, M.; Glenn, A. G.; Weakley, T. J. R.; Tyler, D. R. *Macromolecules* **1999**, *32*, 3898−3906.
(11) Adams, R. D.; Cotton, F. A. *Inorg. Chim. Acta* **1973**, *7*, 153−156.
(12) Adams, R. D.; Collins, D. M.; Cotton, F. A. *Inorg. Chem.* **1974**, *13*, 1086−1090.
(13) Linehan, J. C.; Yonker, C. R.; Bays, J. T.; Autrey, S. T. *J. Am. Chem. Soc.* **1998**, *120*, 5826−5827.
(14) Linehan, J. C.; Wallen, S. L.; Yonker, C. R.; Bitterwolf, T. E.; Bays, J. T. *J. Am. Chem. Soc.* **1997**, *119*, 10170−10177.
(15) Franz, J. A.; Linehan, J. C.; Birnbaum, J. C.; Hicks, K. W.; Alnajjar, M. S. *J. Am. Chem. Soc.* **1999**, *121*, 9824−9830.
(16) Autrey, S. T.; Devadoss, C.; Suerwien, B.; Franz, J. A.; Schuster, G. B. *J. Phys. Chem.* **1995**, *99*, 869−871.

10.1021/om000724j CCC: $20.00
Publication on Web 01/05/2001

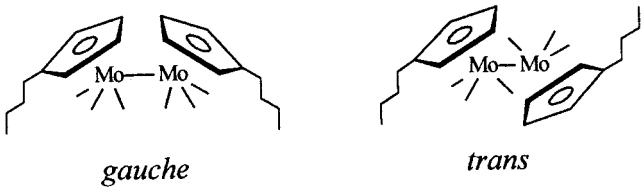

Figure 1. Schematic representations of the *gauche* and *trans* rotomers of $[(n\text{-butylCp})Mo(CO)_3]_2$.

have examined the radical recombination rates of $(n\text{-butylCp})Mo(CO)_3$ in four dissimilar solvents using step-scan FTIR spectroscopy. We have chosen the monobutyl–cyclopentadienyl derivative $(n\text{-butylCp})Mo(CO)_3$ to initiate investigations into the differences of the radical self-termination rate between substituted and nonsubstituted cyclopentadienyl ligands. The phosphine-for-carbonyl substitution in the manganese pentacarbonyl radical, $Mn(CO)_4L$ (L is phosphine), significantly slows the radical self-termination rate. For this radical the rate of self-termination was inversely proportional to the cone-angle of the phosphine.[18] The $CpCr(CO)_3$ and $Cp^*Cr(CO)_3$ (Cp* is pentamethyl-η^5-cyclopentadienyl) radical systems have been compared, with the $Cp^*Cr(CO)_3$ self-termination rate being 40 times slower than $CpCr(CO)_3$.[19] But in the chromium system the rate constants for radical recombination are much slower than the diffusion- or near diffusion-controlled rates reported for both the molybdenum and tungsten radicals.

The addition of a butyl side chain to the cyclopentadienyl ring also has the benefit of increasing the solubility of the organometallic compound. The alkyl side chain increases the solubility of the organometallic radical complex in nonpolar solvents such as aliphatics and CO_2. The solubility of the hydride, $R_5CpMo(CO)_3H$ (a model for the $R_5CpMo(CO)_3$ radical), significantly increased in dodecane when R is methyl as opposed to R being hydrogen.[15]

In this study we present our preliminary results into the investigations of organometallic radical self-termination rates as a function of viscosity over a large viscosity range through the use of compressible gases and noncompressible liquids. We also report the first rates for radical-to-*gauche* isomerization. Future experimental efforts will examine the organometallic radical self-termination rates based on radical size as a function of temperature, pressure, and viscosity for both liquids and compressible gas solvents.

Results

Figure 2 shows the FTIR spectra of $[(n\text{-butylCpMo}(CO)_3]_2$ at 283 K in the four solvents used in this study. The IR spectra in heptane, CO_2, and xenon are all very similar with only a slight band broadening apparent in the CO_2 spectrum. The IR spectrum of the molybdenum dimer in THF shows a significant amount of *gauche* rotamer, band maximum at 2018 cm^{-1}. The *gauche*-$[(n\text{-butylCpMo}(CO)_3]_2$ rotamer shows an equilibrium concentration of 20% by ^1H NMR in THF.[20] This is consistent with the previously reported *gauche*-to-*trans* ratio for $[CpMo(CO)_3]_2$ in acetone of approximately 1:1, with the ratio in THF being slightly smaller.[11,12] In heptane the amount of *gauche*-$[(n\text{-butylCpMo}(CO)_3]_2$ was undetectable by ^1H NMR (<1%). At extremely high resolution and long optical path length, the static IR spectrum of $[(n\text{-butylCp})Mo(CO)_3]_2$ in heptane does show a small band at 2015 cm^{-1}, which may correspond to a very small amount of *gauche* rotamer.[21]

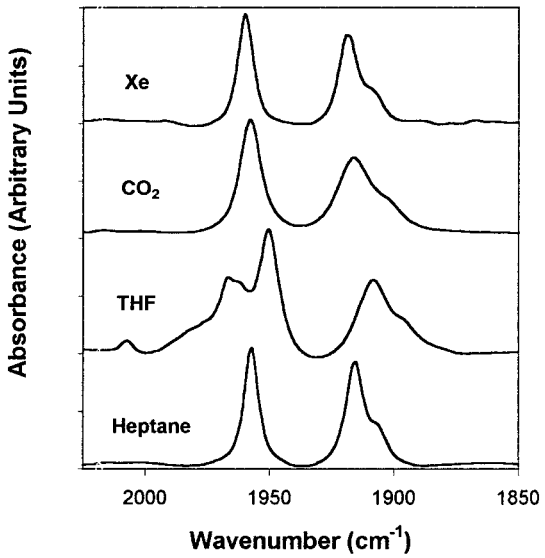

Figure 2. FTIR spectra of $[(n\text{-butylCp})Mo(CO)_3]_2$ solutions in xenon, carbon dioxide, tetrahydrofuran, and *n*-heptane collected at 8 cm^{-1} resolution.

Photolysis of $[(n\text{-butylCp})Mo(CO)_3]_2$ was performed at 532 nm to produce the $(n\text{-butylCp})Mo(CO)_3$ radical, eq 1. Figure 3 shows typical step-scan FTIR time slices for the $[(n\text{-butylCpMo}(CO)_3]_2$ system photolyzed at 532 nm in heptane. The negative band at 1957 cm^{-1} and the positive bands at 2005 and 2015 cm^{-1} were used to quantify the *trans*, radical, and *gauche* species, respectively. Notice that immediately after the laser flash, t_o, the only positive bands are due to the radical at 2005 and 1905 cm^{-1}. The radical and the *gauche* rotamer have essentially equal intensities at 1 μs after the laser pulse. After 50 μs there is little contribution from the radical to the shoulder of the *gauche* band at 2015 cm^{-1}. The spectral region between 1880 and 1950 cm^{-1} is extremely complex with positive contributions to the spectral intensity in this region from the radical and the *gauche* isomer and negative contributions from the *trans* isomer. There are no observable bands in this spectral region due to the pentacarbonyl species, $[(n\text{-butylCp})Mo(CO)_2(\mu^2\text{-CO})(n\text{-butylCp})Mo(CO)_2]$, which are present at higher energy irradiation (e.g., 355 nm).[7]

$$[(n\text{-butylCp})Mo(CO)_3]_2 \xrightarrow{h\nu} 2(n\text{-butylCp})Mo(CO)_3 \quad (1)$$

Reaction pathways for radical recombination are summarized in Scheme 1. The $(n\text{-butylCp})Mo(CO)_3$

(17) Camaioni, D. M.; Autrey, S. T.; Salinas, T. B.; Franz, J. A. *J. Am. Chem. Soc.* **1996**, *118*, 2013–2022.
(18) Walker, H. W.; Herrick, R. S.; Olsen, R. J.; Brown, T. L. *Inorg. Chem.* **1984**, *23*, 3748–3752.
(19) Yao, Q.; Bakac, A.; Espenson, J. H. *Organometallics* **1993**, *12*, 2010–2012.
(20) The NMR spectrum was obtained in d_8-THF or d_{16}-heptane at 283 K on a Varian VXR-300.
(21) This band may also be due to a small unallowed transition of the *trans* isomer.

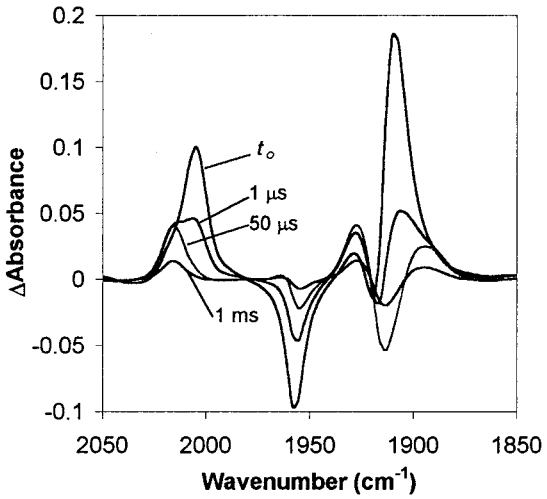

Figure 3. Transient FTIR time-slice spectra of [(*n*-butylCp)Mo(CO)$_3$]$_2$ photolyzed at 532 nm in heptane at 283 K. Immediately after photolysis, t_o, the large positive peaks at 2005 and 1900 cm^{-1} are due to the (*n*-butylCp)Mo(CO)$_3$ radical and the large negative peaks from the bleaching of *trans*-[(*n*-butylCp)Mo(CO)$_3$]$_2$. At 1 μs the *gauche*-[(*n*-butylCp)Mo(CO)$_3$]$_2$ and the radical have comparable peak intensities. At 1 ms only the *gauche*-[(*n*-butylCp)Mo(CO)$_3$]$_2$ is visible in the 2000 cm^{-1} region.

Scheme 1

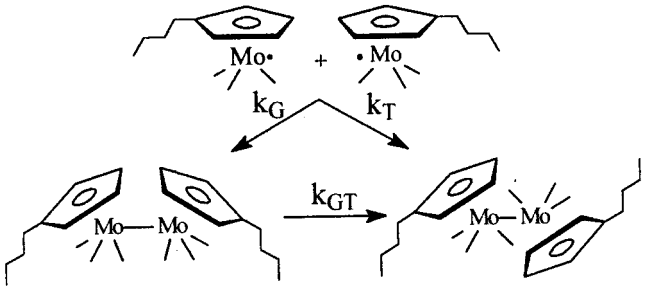

radical can recombine to either the *gauche*- or the *trans*-[(*n*-butylCp)Mo(CO)$_3$]$_2$ dimers. The *gauche* isomer subsequently isomerizes to the *trans* rotamer since the *gauche* rotamer is produced in higher than equilibrium concentrations by radical recombination. The overlap between the *gauche* and the radical bands in the 2000−2020 cm^{-1} region of the IR spectrum makes careful deconvolution of the two bands necessary to obtain accurate rate constants using accurate molar absorptivity values. At times long after the initial photolysis pulse (>200 μs) the contributions of the radical to the intensities in the IR spectrum in the 2000−2020 cm^{-1} region are small relative to those of the *gauche* dimer. If, as is observed in this study, there are no other species formed and the system returns to equilibrium before the next laser pulse, then the mass balance is denoted in eq 2.[22]

$$-[trans]_{\text{bleached}} = [\text{radical}]/2 + [gauche] \qquad (2)$$

When the [radical] ≪ [*gauche*], which occurs at long observation times, then [*gauche*] = −[*trans*]$_{\text{bleached}}$. This allows the determination of the molar absorptivities for the *gauche* transient. The radical molar absorptivity is determined from a fit of the mass balance, eq 2, over the entire time range once the molar absorptivity of *gauche* transient has been determined. The molar absorbtivities determined for the three species at 8 cm^{-1} resolution are presented in the Supporting Information table. The concentration profiles over time for these species in heptane at 283 K determined by the above method are shown in Figure 4. Similar profiles were obtained for the other three solvents in this study. The mass balance determined from this analysis is very good, with less than a 1% deviation from zero over the entire time range in each of the solvents except xenon, in which a 2% deviation was found.

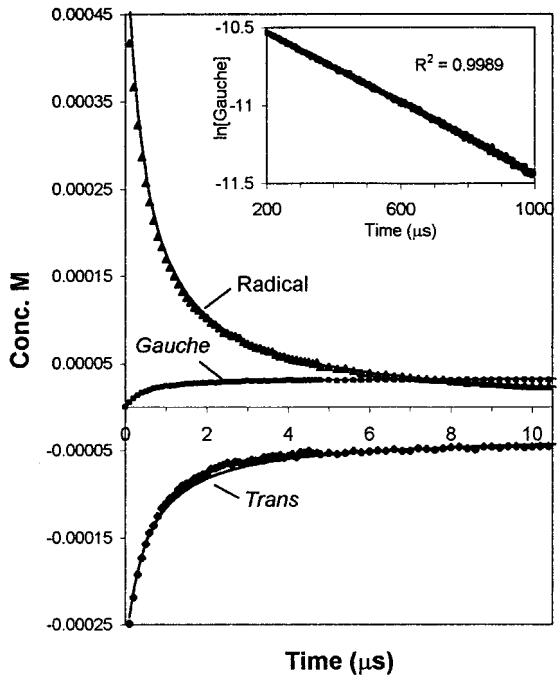

Figure 4. First 10 μs of the concentration profile vs time for radical (*n*-butylCp)Mo(CO)$_3$, *trans*-[(*n*-butylCp)Mo(CO)$_3$]$_2$, and *gauche*-[(*n*-butylCp)Mo(CO)$_3$]$_2$ species at 283 K in heptane. The solid lines represent the Levenberg−Marquardt fit of the data. The inset shows the linear plot of ln[*gauche*-[(*n*-butylCp)Mo(CO)$_3$]$_2$] against time after most of the radical has decayed. Notice the difference in the time scales between the two plots.

A more complicated three-part deconvolution was used to determine the molar absorptivity for the radical band at 1905 cm^{-1} in THF since a solvent band interferes with the quantification of the radical band at 2000 cm^{-1}. This complication leads to a greater uncertainty in the THF results when compared to the other solvents. The molar absorptivities of the other species in THF were obtained in a manner similar to that for the other solvents as described above.

The rate constants for the reactions were determined by nonlinear least-squares fit of the concentrations of each species using approximations to the analytical solutions of the differential equations, eqs 3−5 (shown below), via the Levenberg−Marquardt technique. The rate constants determined in heptane, along with those obtained in xenon, THF, and CO_2, are shown in Table 1.

(22) There is a very small IR band at 1667 cm^{-1} observed in these experiments. This corresponds to the pentacarbonyl dimer intermediate at a concentration of less than 0.5% of the *trans* bleached. The absorbances due to this species are negligible in the 1963 cm^{-1} region used for *trans* quantification. The 1667 cm^{-1} band grows in intensity proportional with reaction temperature.

Table 1. Rate Constants for the [(*n*-butylCp)Mo(CO)$_3$]$_2$ Photolyzed Systems at 283 K[a]

	solvent			
rate constant	heptane	xenon	CO_2	THF
$2k_R$ (M^{-1} s^{-1})	$(3.2 \pm 0.5) \times 10^9$	$(7.9 \pm 0.5) \times 10^9$	$(1.7 \pm 0.5) \times 10^9$	$(2.2 \pm 0.8) \times 10^9$
$2k_R$[b] (M^{-1} s^{-1})	3.2×10^9	7.7×10^9	1.6×10^9	2.3×10^9
k_T (M^{-1} s^{-1})	$(1.5 \pm 0.5) \times 10^9$	$(3.5 \pm 0.5) \times 10^9$	$(0.70 \pm 0.1) \times 10^9$	$(0.84 \pm 0.3) \times 10^9$
k_G (M^{-1} s^{-1})	$(0.10 \pm 0.07) \times 10^9$	$(0.32 \pm 0.07) \times 10^9$	$(0.13 \pm 0.07) \times 10^9$	$(0.23 \pm 0.2) \times 10^9$
k_{GT} (s^{-1})	$(1.1 \pm 0.1) \times 10^3$	$(1.0 \pm 0.1) \times 10^3$	$(0.91 \pm 0.05) \times 10^3$	$(1.0 \pm 0.05) \times 10^3$
k_{GT}[c] (s^{-1})	1.1×10^3	1.1×10^3	0.88×10^3	0.96×10^3
k_T/k_G	15	11	5.4	3.7
$k_R/(k_G + k_T)$[d]	1.005	1.006	1.019	1.016

[a] Uncertainties are estimates of 2σ. A major source of uncertainty comes from the uncertainties in the molar absorptivities. [b] Linear fit of 1/[R] vs time. [c] Linear fit of ln[G] vs time. [d] $k_R/(k_G + k_T)$ should equal 1 and is another check of the correctness of the fit.

$$\frac{d[R]}{dt} = -2k_R[R]^2 \quad (3)$$

$$\frac{d[G]}{dt} = k_G[R]^2 - k_{GT}[G] \quad (4)$$

$$\frac{d[T]}{dt} = k_T[R]^2 + k_{GT}[G] \quad (5)$$

where R = (*n*-butylCp)Mo(CO)$_3$, G = *gauche*-[(*n*-butylCp)Mo(CO)$_3$]$_2$, and T = *trans*-[(*n*-butylCp)Mo(CO)$_3$]$_2$.

The overall rate constant for radical recombination, $2k_R$, could also be determined by a linear graphical fit of 1/[R] vs time, as shown in Figure 5. The first-order rate constant, k_{GT}, for the isomerization of *gauche*-to-*trans* could also be obtained from a linear fit of ln[G] vs time after the radical concentration approaches zero (see inset in Figure 4). These graphical solutions are also presented in Table 1 for comparison with the values derived from nonlinear least-squares fit to the differential equations. The $2k_R$ and the k_{GT} values obtained by the two methods yield almost identical results.

The use of the differential analysis to calculate the rate constants not only yielded the overall rate constant for radical recombination, $2k_R$, but also yielded the individual rates of formation of the *gauche* dimer, k_G, and the *trans* dimer, k_T, from the radical. From Table 1 we can see that the rate of recombination of the radical to form the *trans* isomer is much faster than *gauche* formation. The last row in Table 1 shows another fit parameter, $k_R/(k_G + k_T)$. Since the values for the rate constants were determined independently, the good agreement, <2% in all cases, of this parameter again supports the accuracy of the analysis method.

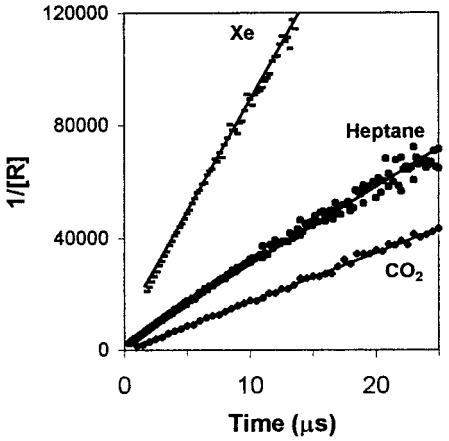

Figure 5. Plots of 1/[(*n*-butylCp)Mo(CO)$_3$] as a function of time showing the linear relationship. The solid line is the linear least-squares fit for the data range shown.

Table 2. Selected Solvent Parameters for the Solvents Investigated

solvent	dielectric constant	density (g/mL)[a]	viscosity (cP)[a]	T_c (K)
heptane	1.92[b]	0.693[c]	0.466[c]	540.2[c]
xenon	1.54[d]	2.42[e]	0.193[e]	289.5[c]
CO_2	1.53[d]	1.04[e]	0.153[f]	304.3[c]
THF	7.52[b]	0.815[c]	0.580[c]	540.2[c]

[a] At 283 K. [b] *CRC Chemical Handbook of Chemistry and Physics*, 63rd ed.; Weast, R. C., Astle, M. J., Eds.; CRC Press, Inc.: Boca Raton, 1983. Dielectric constants are quoted for 293 K. [c] Reid, R. C.; Prausnitz, J. M.; Sherwood, T. K. *The Properties of Liquids and Gases*, 3rd ed.; McGraw-Hill: New York, 1977. [d] Bose, T. K. In *Dielectric Properties of Dense Fluids*; Tabisz, G. C., Neuman, M. N., Eds.; Kluwer Academic Publishers: Amsterdam, 1995; pp 77−86. [e] *Handbook of Physical Properties of Liquids and Gases*, 3rd ed.; Varagaftik, N. B., Vinogradov, Y. K., Yargin, V. S., Eds.; Begell House Inc.: New York, 1996. [f] NIST Standard Reference Database 23, "NIST Thermodynamic and Transport Properties of Refrigerants and Refrigerant Mixtures−REFPROP", McLinden, M. O.; Klein, S. A.; Lemmon, E. W.; Peskin, A. P. 1998.

Discussion

Rates of Recombination. We have chosen four dissimilar solvent systems to investigate solvent effects on the rates of organometallic radical reactions. The reaction temperature, 283 K, was chosen to allow each of the solvents to be studied in their liquid state; the critical temperature, T_c, of xenon is 289.5 K and T_c for CO_2 is 304.3 K. The low 283 K temperature also reduces the CO loss from the dimer due to thermal or photothermal effects, which allows a more accurate mass balance.[22] Table 2 shows some of the properties of the solvents used in this study.

The overall rate constants, $2k_R$, for radical self-termination in xenon, heptane, and THF follow the expected diffusion-controlled reaction trend, with $2k_R$ increasing with decreasing viscosity; see Figure 6. The notable exception for this trend is the rate constant, 1.7×10^9 M^{-1} s^{-1}, determined in CO_2. Liquid CO_2 used in this study has the lowest viscosity of any solvent used for an organometallic radical self-termination study. The expected $2k_R$ value should be much faster than 1×10^{10} M^{-1} s^{-1} if the rate was strictly diffusion controlled. For example, the measured $2k_R$ for this radical recombination in xenon at 138 bar and 283 K (corresponding to a viscosity lower than for CO_2 at 350 bar and 283 K, 0.144 vs 0.153 cP) was determined to be $(3 \pm 2) \times 10^{10}$ M^{-1} s^{-1}.

One explanation for the slow self-termination rate in CO_2 may be a competing equilibrium step in which the organometallic radical binds, either covalently or through

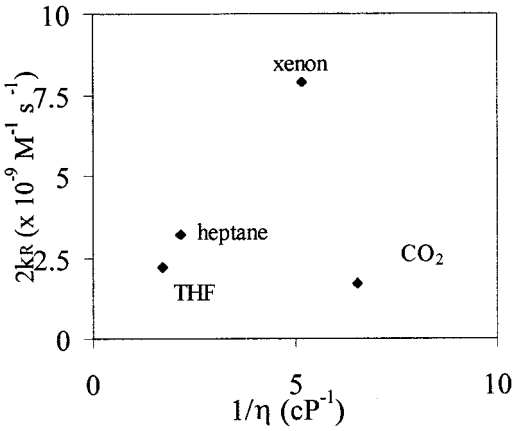

Figure 6. Overall radical recombination rate, $2k_R$, plotted against 1/viscosity. This plot shows that the rate constants increase with decreasing viscosity except for CO_2.

a van der Waals complex, to the solvent, eq 6. This has been suggested for other ligating solvents such as THF and acetonitrile with $CpMo(CO)_3$.[2]

$$(n\text{-butylCp})Mo(CO)_3 + CO_2 \leftrightarrow (n\text{-butylCp})Mo(CO)_3(CO_2) \quad (6)$$

The existence of transient 19-electron organometallic complexes has been deduced based on reaction products.[3,4,23,24] The $CpMo(CO)_3(CO_2)$ 19-electron organometallic complex has been proposed on the basis of transient IR band analysis.[25] While we do not observe the proposed shoulder near 1905 cm^{-1} attributed to the radical CO_2 complex, our kinetics are consistent with such a complex.

The persistent radical NO has been observed to form a NO−CO_2 radical van der Waals complex.[26] While the size and the mass of a (*n*-butylCp)$Mo(CO)_3$−CO_2 complex may not be much different than the naked (*n*-butylCp)$Mo(CO)_3$ radical, a CO_2 van der Waals complex may reduce the diffusion rate of the organometallic radical in CO_2 enough to yield a slower rate of termination, $2k_R$. This would be consistent with the results from organic radical chemistry in which organic radicals which can interact with the solvent (such as polar radicals in polar solvents) have slower recombination rates than in nonreacting solvents.[27] The diffusion rate for the (*n*-butylCp)$Mo(CO)_3$−CO_2 complex would have to be much slower than for (*n*-butylCp)$Mo(CO)_3$ if $2k_R$ determined in CO_2 is less due solely to a slower diffusion rate.

The overall rate constant for the radical recombination, k_R, in heptane at 283 K for (*n*-butylCp)$Mo(CO)_3$ at 1.6×10^9 M^{-1} s^{-1} is slower than for $CpMo(CO)_3$, 3×10^9 M^{-1} s^{-1} at 298 K in heptane, [6] or 3.4×10^9 M^{-1} s^{-1} for $CpMo(CO)_3$ in toluene at 298 K,[28] 3.9×10^9 M^{-1} s^{-1} at 296 K in acetonitrile,[19] or 3.1×10^9 M^{-1} s^{-1} in cyclohexane at 295 K.[2,29] The previously reported values for room-temperature reactions are nearly equivalent within their respective uncertainties, but the viscosity of the solvents studied varies from 0.397 cP for heptane at 298 K to 0.960 cP for the original cyclohexane work. It is generally accepted, and has been shown for a number of organic radicals, that the radical recombination rate is proportional to temperature/viscosity (T/η).[30] The previously reported rate constants for $CpMo(CO)_3$ do not appear to follow the T/η trend observed for organic radicals. This could be due to the extreme difficulty in the measurement (solvent impurities such as olefins or small amounts of O_2 can lead to faster apparent rates when direct observation of the radical is employed).

The different measurement techniques utilized may also influence the final rate constant obtained. Infrared bands were used in one determination, while UV−visible bands were used in the other measurements. The latter measurement technique has hidden pitfalls in light of the *gauche*/*trans* nonzero equilibrium in solvents with high dielectric constants such as THF and aceonitrile. Knorr and Brown have shown that the visible absorption of *gauche*- and *trans*-$[CpMo(CO)_3]_2$ have different maxima in the visible and the UV (in toluene: *gauche*-$[CpMo(CO)_3]_2$ λ_{max} at 362 and 450 nm; *trans*-$[CpMo(CO)_3]_2$ λ_{max} at 389 and 525 nm).[7] Irradiation into one or the other band may lead to preferential photolytic depletion of either the *gauche* or *trans* rotamers.

The differences in visible absorption maxima for the *gauche* and the *trans* rotamers can also lead to difficulties in measuring the concentrations of each species after photolysis. The observed absorbances at some wavelengths may be a combination of contributions from both isomers, which have different molar absorptivities. An accurate rate determination would need to address the contribution of the *gauche* rotamer formed due to radical recombination to the absorbance at the *trans* observation wavelength. This is especially important based on our reported solvent-dependent *gauche*-to-*trans* kinetic ratios (see below).

We are currently investigating the solvent dependence on the radical self-termination rate in all solvents as a function of temperature (viscosity) and, where appropriate, pressure. The differences in the rate dependence on viscosity in individual solvents will allow a better understanding of the factors affecting organometallic radical self-termination.

Rates of Formation of *Trans* and *Gauche* Isomers. The rate of formation of the *gauche* isomer from the radical is slower than the rate of *trans* formation in each of the solvents studied as shown in Table 1. The rates of formation of the *trans* and *gauche* rotamers from the radical yield insights into the processes governing organometallic radical recombination. If the recombination rates were strictly diffusion controlled, one would expect the *trans*-to-*gauche* rate ratio for the reformation of the dimer from the radical to be near 1. As can be seen from Table 1, the ratio k_T/k_G is much greater than 1. The thermodynamics of the system suggests that the k_T/k_G ratio should be equal to the equilibrium constant, K_{eq}, for [*trans*]/[*gauche*]. But, the self-termination of the

(23) Mao, F.; Philbin, C. E.; Weakley, T. J. R.; Tyler, D. R. *Organometallics* **1990**, *9*, 1510−1516.
(24) Zavarine, I. S.; Kubiak, C. P. *Coord. Chem. Rev.* 1998, *171*, 419−438.
(25) George, M. W.; Grills, D. C.; Sun, X.-Z.; Poliakoff, M. *Stud. Surf. Sci. Catal.* **1998**, *114*, 255−260.
(26) Zhou, M.; Zhang, L.; Qin, Q. *J. Am. Chem. Soc.* **2000**.
(27) Lehni, M.; Fischer, H. *Int. J. Chem. Kinetics* **1983**, *15*, 733−757.
(28) Vlierberge, B. A. v.; Abrahamson, H. B. *J. Photochem. Photobiol.* **1990**, *52*, 69.
(29) Hughey, J. L.; Bock, C. R.; Meyer, T. J. *J. Am. Chem. Soc.* **1975**, *97*, 4440.
(30) Fischer, H.; Paul, H. *Acc. Chem. Res.* **1987**, *20*, 200−206.

radical yields a nonequilibrium distribution of *trans*- and *gauche*-[(*n*-butylCp)CpMo(CO)$_3$]$_2$, as is evident by the appearance of *gauche* (which in heptane, CO_2, and xenon has a near-zero equilibrium concentration) and by the thermal isomerization of the *gauche* into *trans* in all solvents. The ratio of the rate constants for the formation of *gauche*-[(*n*-butylCp)Mo(CO)$_3$]$_2$, k_G, and *trans*-[(*n*-butylCp)Mo(CO)$_3$]$_2$, k_T, k_T/k_G, appears to be solvent dependent. This ratio is smallest in THF and largest in heptane.

The NMR and FTIR spectroscopies demonstrate that the equilibrium concentrations of the *gauche* isomer are small. At thermal equilibrium, the *gauche*-[(*n*-butylCp)-Mo(CO)$_3$]$_2$ isomer could not be seen by ^{1}H NMR in either heptane or CO_2. This negative observation of the *gauche* isomer by ^{1}H NMR leads to a maximum amount of *gauche*-[(*n*-butylCp)Mo(CO)$_3$]$_2$ present in these solvents at less than 5%, more likely less than 2%, of the total dimer concentration. The equilibrium constant [*trans*]/[*gauche*] must be greater than 20 for these solvents. No ^{1}H NMR experiment was conducted in xenon, but based on the similar dielectric constants for xenon, CO_2, and heptane we expect a similar equilibrium *gauche* concentration. Static high-resolution FTIR spectroscopy of heptane and xenon solutions show a band that could correspond to *gauche*-[(*n*-butylCp)Mo(CO)$_3$]$_2$.[21] The concentration of *gauche*-[(*n*-butylCp)Mo(CO)$_3$]$_2$ is less than 1% when the extinction coefficient for *gauche*-[(*n*-butyl-Cp)Mo(CO)$_3$]$_2$ determined during the step-scan FTIR experiments was used. This leads to an estimation of K_{eq} greater than 99. The band at 2015 cm^{-1} observed using static FTIR in CO_2 is less than 0.5% of the total dimer concentration at 283 K.

THF is a unique solvent in this study because it has a large equilibrium concentration of *gauche*-[(*n*-butyl-Cp)Mo(CO)$_3$]$_2$ ([*trans*]/[*gauche*] = 4) present in solution at 283 K. The ratio k_T/k_G obtained in THF, 3.7, is very near the equilibrium [*trans*]/[*gauche*] ratio of 4 determined by proton NMR. The k_T/k_G ratios for the other three solvents in this study vary from 5.4 to 15. The value of 5.4 obtained in CO_2 corresponds to a *gauche*-[(*n*-butylCp)Mo(CO)$_3$]$_2$ concentration of over 8% which would have been detected in the proton NMR if the *gauche* isomer was present at this concentration at equilibrium. Therefore the k_T/k_G values obtained in CO_2, heptane, and xenon do not correspond to the equilibrium constant between *trans* and *gauche*.

The k_T/k_G ratio for the solvents other than THF may be a manifestation of the radical cage lifetime in each solvent. The longer the radicals remain in the solvent cage, the more molecular rotation may occur which can approach the equilibrium value of [*trans*]/[*gauche*] for that solvent. The values of k_T/k_G obtained in the three solvents with very low *gauche* equilibrium concentrations (heptane, CO_2, and xenon) correlate well with $1/\eta$, while THF does not.[31] An alternative explanation of the varying k_T/k_G ratios with solvent may be a more favorable steric environment inside the radical cage for the radicals oriented in a *trans* configuration prior to bond formation. The butyl groups on the Cp ligand may cause enough steric repulsion to favor the *trans* isomer.

***Gauche*-to-*Trans* Isomerization.** The rate of isomerization from *gauche*-to-*trans*-[(*n*-butylCp)Mo(CO)$_3$]$_2$ does not change with solvent. The rate constants, k_{GT}, obtained in the four solvents are all clustered about 1000 s^{-1}, with the value determined in CO_2 being slightly lower than the other three solvents. This rate constant appears to be independent of solvent viscosity, as expected for a non diffusion controlled reaction. Rate constants obtained for the isomerization of *gauche*-[CpMo(CO)$_3$]$_2$ to *trans*-[CpMo(CO)$_3$]$_2$ at 293 K (k_{GT} = 300 s^{-1} in heptane) and at 274 K (k_{GT} = 2.6 s^{-1} in DMF) are slower than the *n*-butylCp derivative at 283 K.[6,7,32] The faster isomerization rate for the butyl derivitive is most likely due to less favorable thermodynamics for the *gauche* isomer in the *n*-butyl-substituted dimer than for the nonsubstituted dimer, caused by steric repulsion of the *n*-butyl groups in the *gauche* isomer. The thermodynamic driving force is evidenced in THF by the lower value for *gauche*/*trans* equilibrium found in the nonderivatized cyclopentadienyl dimer, K_{eq} = 1.2, than for the *n*-butyl-substituted dimer, K_{eq} of approximately 4. A temperature study is needed to extract the activation parameters for this isomerization.

Conclusions

We have shown that the rate of organometallic radical recombination follows the expected inverse viscosity relationship in heptane, xenon, and THF, but not in CO_2. In heptane, THF, and xenon the rates of (*n*-butylCp)Mo(CO)$_3$ recombination increase with decreasing density. In CO_2 the (*n*-butylCp)Mo(CO)$_3$ radical may be in equilibrium with a (*n*-butylCp)Mo(CO)$_3$−CO_2 solvent complex. We have also observed that while the thermodynamically more stable *trans* isomer is preferentially formed over the *gauche*, there is a nonequilibrium production of the *gauche* isomer from radical pair recombination. The ratio of the *gauche* and *trans* formation rates, k_T/k_G, appears to vary with solvent. This study provides rate constants necessary for further kinetic and thermodynamic studies of metal radical systems without the need to calculate rate constants (see for example ref 15, in which the radical recombination rate constant is necessary for the accurate determination of Arrhenius parameters of the hydrogen atom abstraction by benzyl radical from a molybdenum hydride).

We have begun this study of the RCpMo(CO)$_3$ radical system to determine the total reaction path and temperature/pressure-dependent rate constants for the whole suite of reactions of this radical system. The present work lays the groundwork for more interrogations of the organometallic radical system such that the factors affecting organometallic radical self-termination reactions may be elucidated. The pressure/temperature relationships for the (RCp)Mo(CO)$_3$ radical rates in these and other solvents are currently under investigation.

Experimental Section

Sample Preparation. The [(*n*-butylCpMo(CO)$_3$]$_2$ dimer was synthesized by published procedures and recrystallized from pentane at low temperatures prior to use.[33,34] The *n*-heptane (Aldrich, HPLC grade) was washed successively with concentrated sulfuric acid, acidic potassium permanga-

(31) Preliminary results in dodecane show a k_T/k_G ratio of over 20 at a viscosity of 1.9 cP.

(32) Chen, X.; Mann, B. E. *Organometallics* **1996**, *15*, 3703−3707.

nate solution, and water.[35] The heptane was dried by distilling from sodium and freeze−pump−thaw degassed. The THF used in this study (Aldrich, HPLC grade) was distilled from sodium benzophenone and degassed prior to use. The xenon (Spectra Gases, Inc) and CO_2 (Scott Speciality Gases, ScF Grade) gases were used as received.

Liquid solvent samples were prepared in an inert atmosphere box and placed in a stainless steel cylinder, which was then pressurized with 500 psi of He. To eliminate oxygen, the pumps, tubing, and optical cell were purged and vented with N_2 (500−20 psi) a minimum of five times before the sample was flushed into the feed pump using the backpressure in the steel sample cylinder. Liquid samples prepared this way were found to be stable for at least 2 weeks. The pressure and flow were controlled by operating the Varian feed pump (Model 8500) in constant pressure mode and a similar Varian receiving pump operating in constant flow mode. The flow of 1 mL/min flushed the optical cell volume approximately 20 times per minute. A backpressure of 1100 psi was used to ensure the liquid samples remained oxygen free.

For samples using a compressible fluid for the solvent (CO_2, Xe) an Isco syringe pump (Model 260D) was used to transfer the liquid fluid (400 bar, 5 °C) to the Varian feed pump. A 3 mL Supleco extraction cell (Model #5-7389) was placed inline between the Isco pump and Varian fed pump. Measured quantities of [(*n*-butylCpMo$(CO)_3$]$_2$ placed in the extraction cell were swept into the feed pump while it filled with liquid CO_2 or Xe. To eliminate oxygen, the system was purged with CO_2 or Xe in the same method described for liquid samples. Samples prepared this way were found to be stable for more than a month.

Temperature was controlled (±0.1 °C) with a VWR Model 1146 chiller, providing flow to both the optical cell and a thermal equilibration coil consisting of 1 m of stainless steel tubing (1/16-in. o.d. × 0.03-in. i.d.) in a copper block. The coil was placed immediately before the optical cell to ensure that the solution had reached the desired temperature prior to entering the cell.

IR Spectroscopy. Spectral data was collected with a Bruker Model IFS66 spectrophotometer controlled with a 586 PC and Bruker OPUS software. Static IR spectra were acquired using the dc channel of a Kolmar Technologies HgCdTe dual channel detector (Model KMPV11-1-LJ2). The IR beam aperture was adjusted to fill the optical cell window to facilitate uniform sample interrogation. Dynamic IR, or time-resolved IR (TRIR) spectra were acquired by operating the Bruker spectrophotometer in step-scan mode. For TRIR spectroscopy both the ac and dc channels of the of Kolmar HgCdTe detector were utilized. The laser-induced TRIR signal was acquired from the ac coupled detector channel while the proper phase correction was determined from the detectors' dc signal. Since the laser-induced changes in the interferogram are very small, the ac signal was amplified with a Stanford Research Model 445. Output from both detector channels was processed with a Bruker 200 MHz PAD 82A digitizer (2 channels, 8 bit, 20 MB).

Unless otherwise stated, TRIR spectra were collected with 8 cm^{-1} resolution, 20 coadditons, 2 levels zero-filling, Mertz (no peak search) phase correction, and Blackman Harris 3 term apodization function. Static reference spectra were collected (through the PAD 82A) before and after TRIR data collection. A 4.78−6.25 μm (Laser Components GmbH F301-4) band-pass filter was used to isolate the spectral region of interest (2100−1600 cm^{-1}) and reduce the number of interferogram measurement points required. Multiple time slice data were collected for each solvent and the results combined for data analysis.

Sample concentrations were adjusted to keep the sample absorbance at the photolysis wavelength below 0.1 to ensure uniform photolysis and avoid concentration gradients. Nonlinear response regions with $A \geq 1$ were avoided for both static IR and TRIR data.

The optical cell was a high-pressure Wilmad flow cell (Model #118-1P-2-SP2) with 13 × 6 mm CaF_2 windows. Custom stainless steel spacers, designed to minimize dead volume and promote laminar flow, were used between the CaF_2 windows.

For photolysis, the second harmonic (532 nm) of a Continuum Surelite Nd:YAG laser, operating at 10 Hz and 25 mJ/pulse, was used. The laser beam diameter exceeded the optical cell aperture, ensuring uniform photolysis irradiance with 50% of the laser energy entering the sample. A Stanford Research pulse generator (Model DG535) provided accurate, coordinated triggering for the digitizer, laser flashlamp, and laser Q-switch.

Data Analysis. The t*rans*-[(*n*-butylCpMo$(CO)_3$]$_2$ dimer molar absorptivity was measured statically, allowing concentration profiles of this species to be directly determined from TRIR data. The molar absorptivities of the transient species cannot be directly measured and must be indirectly calculated. Even using a spectral resolution of 4 cm^{-1}, the g*auche*-[(*n*-butylCpMo$(CO)_3$]$_2$ (∼2015 cm^{-1}) and radical bands (∼2005 cm^{-1}) overlap significantly. A multicomponent deconvolution (two bands, two species) was applied to each spectrum to get species-specific absorbance as a function of time. Relative absorptivities of the two overlapping species were estimated by examining band shapes in the 2030−1990 cm^{-1} region at very short (<5 μs) and very long times (>400 μs) when only one of the transient species was principally present.

The molar absorptivity for the *gauche* dimer was then determined from the mass balance for the period after most of the radical had recombined. The molar absorptivity for the radical was then determined from the value required to maintain the mass balance (eq 6) as a function of time over the entire time range. The molar absorptivity values of the species were then interactively determined using the generalized reduced gradient method for nonlinear optimization until the mass balance error was minimized over the entire data range.

Concentration profiles were determined from the species molar absorptivities and TRIR absorbance data. Reaction rate constants were determined from the concentration profiles using both the slope of the regression fit to plots of 1/[R] vs time and by analytically solving the differential equations for the rates of disappearance or appearance of the radical, *gauche*, or *trans* species (see eqs 3−5). The rate constants can then be determined by a nonlinear least-squares fit of the experimental data to the analytical solution for each species using the Levenberg−Marquardt technique. The values for the regressed rate constants for the studied solvents are reported in Table 1.

Gauche- to *trans*-[(*n*-butylCpMo$(CO)_3$]$_2$ reconfiguration rate was also determined by exponential regression fit for the period after 99% of the monomer had recombined. The fit was taken over a period of time where the *gauche* concentration fell by at least 80%.

Acknowledgment. This work was supported by the Director, Office of Science, Office of Basic Energy Sciences, Chemical Sciences Division of the U.S. Department of Energy, under Contract DE-ACO6-76RLO 1830.

Supporting Information Available: A table of the molar absorptivities for the transient species in the four solvents and a graph of k_T/k_G vs $1/\eta$ are available. This material is available free of charge via the Internet at http://pubs.acs.org.

OM000724J

(33) Bays, J. T. *Photochemical and Mechanistic Studies of Various Group V and VI Organometallic Compounds in Nujol Matrixes at 77K and in Supercritical Fluids*; Univeristy of Idaho: Moscow, 1998.
(34) Song, L. *Gaodeng Xuexiao Huaxue Xuebao* **1992**, *13*, 1227.
(35) Perrin, D. D.; Armarego, W. L. F.; Perrin, D. R. *Purification of Laboratory Chemicals*, 2nd ed.; Pergamon Press: Oxford, 1980.